ARTICLE

Supporting Information

Multifunctional CuS-CDs@MnO_2 nanoparticles and liposome-Assisted amplification for triple-mode detection of Enrofloxacin

Luna Guo, Huanhuan He, Ruoyan Li, Shiyi Dai, Jing Feng, Guangshuo Zhang, Zixian Li, Weiling Song*, Hong Zhou*

Key Laboratory of Optic-electric Sensing and Analytical Chemistry for Life Science, MOE; Shandong Key Laboratory of Biochemical Analysis; Key Laboratory of Analytical Chemistry for Life Science in Universities of Shandong; College of Chemistry and Molecular Engineering, Qingdao University of Science and Technology, Qingdao 266042, P. R. China

*Corresponding author: Tel.: +86-532-84022700. Fax: +86-532-84022700. Email: shenlan.2003@163.com (Weiling Song); zhouhong@qust.edu.cn (Hong Zhou).

Materials and Reagents

Cholesterol, DSPE-PEG-Mal, tri (2-carboxyethyl) phosphine hydrochloride (TCEP), 1, 2-dioleoacyl-SN-glycerol-3-phosphate choline (DOPC), polyvinylpyrrolidone (PVP) K30), Sodium sulfide 9-hydrate ($Na_2S·9H_2O$), Sodium dihydrogen phosphate (NaH2PO4) and Disodium hydrogen phosphate (Na_2HPO_4) were purchased from Aladdin Reagent (Shanghai, China) Co., Ltd. Streptavidin Magnetic Beads (MB) purchased from Beaver Biotechnology Co., Ltd. Copper chloride dihydrate ($CuCl_2·2H_2O$) and hydrazine hydrate ($N_2H_4·H_2O$) were obtained from Sinopod Chemical Reagent Co., Ltd. Enrofloxacin (ENR), sodium hydroxide (NaOH), hydrochloric acid (HCl) and potassium permanganate ($KMnO_4$) were acquired from Shanghai McLean Biochemical Technology Co., Ltd. (China); All reagents were used as received without additional purification, and all experiments were performed using deionized water produced by the Milli-Q system. Oligonucleotides used in this work were synthesized and purified by Sangon Biotech Co., Ltd. (Shanghai, China). The sequences are listed in Table S1.

Table S1 DNA sequence used in the experiment

Name	Sequences (5'-3')
S1	GTGTTAGCCTAGCCCCCTAAAAAAAAA-Biotin
S2	SH-AAAAAATGAAATAACCCGGGCTCA
Apt	CCCATCAGGGGGCTAGGCTAACACGGTTCGGCTCTCTGAGCCCGGGTTATTTCAGGGGGA

Apparatus.

The morphology of the synthesized products was characterized by transmission electron microscopy (TEM) using a JEM 1200EX microscope (JEOL, Japan), with energy-dispersive X-ray spectroscopy (EDS) also obtained. The hydrated particle size and surface potential were measured using a Nano ZS90 instrument (Malvern Panalytical, USA). X-ray photoelectron spectroscopy (XPS) data were acquired with an ESCALAB 250 spectrometer equipped with a monochromatic X-ray source. X-ray powder diffraction (XRD) patterns were collected on a Shimadzu XRD-6000 diffractometer (Japan). Fluorescence signals and UV-Vis absorption spectra were detected using an F-4600 fluorescence spectrophotometer (Hitachi, Japan) and a U-3010 UV-Vis spectrophotometer (Hitachi, Japan), respectively.

Conjugation of DNA to GSH@Lip and preparation the MB-S1:

The sulfhydryl modified S2 (10 μL, 10 μM) was co-incubated with TCEP (10 mM, 10 μL) for 2 h to reduce the formation of disulfide bonds. 30 μL of GSH@Lip was added and reacted for 8 h at ambient

temperature to obtain the functional GSH@Lip-S2. The unconjugated S2 was removed by centrifugation. Biotin-modified S1 was bound to streptavidin functionalized magnetic beads (MB) through specific recognition of biotin and avidin. Initially, 15 μL of MBs were washed twice in Buffer I and then re-suspended in the Buffer I buffer (100 μL, pH 7.4). S1(10 μL, 10 μM) was added and reacted for 1 h. Then the MB-S1 was obtained after magnetic separation and washing three times with Buffer I.

Photothermal conversion efficiency calculation

The photothermal conversion efficiency (η) could be calculated using equation (1)

$$\eta = \frac{hS(T_{max} - T_{sur}) - Q_{diss}}{I(1 - 10^{-A808})} \quad (1)$$

where h, S and Qdiss are heat transfer coefficient, irradiated area and the baseline energy inputted by the sample cell, Tmax and Tsur are the highest temperature of system and the temperature of surrounding, I and A808 are the power density and absorption of NPs at 808nm respectively.

The value of hS is calculated by using the following equation (2) to (4):

$$hS = \frac{\sum_i m_i C_{p,i}}{\tau_s} \quad (2)$$

$$\tau_s = -ln\theta \quad (3)$$

$$\theta = \frac{T(t) - T_{sur}}{T_{max} - T_{sur}} \quad (4)$$

where m and Cp are the mass of sample and the thermal capacity of sample and t is cooling time after irradiation.

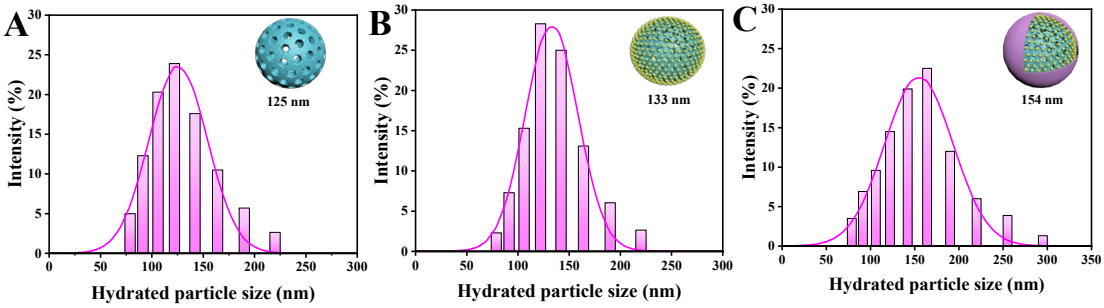

Fig. S1. (A) Particle size distribution of CuS; (B) Particle size distribution of CuS -CDs ; (C) Particle size distribution of CuS –CDs@MnO_2.

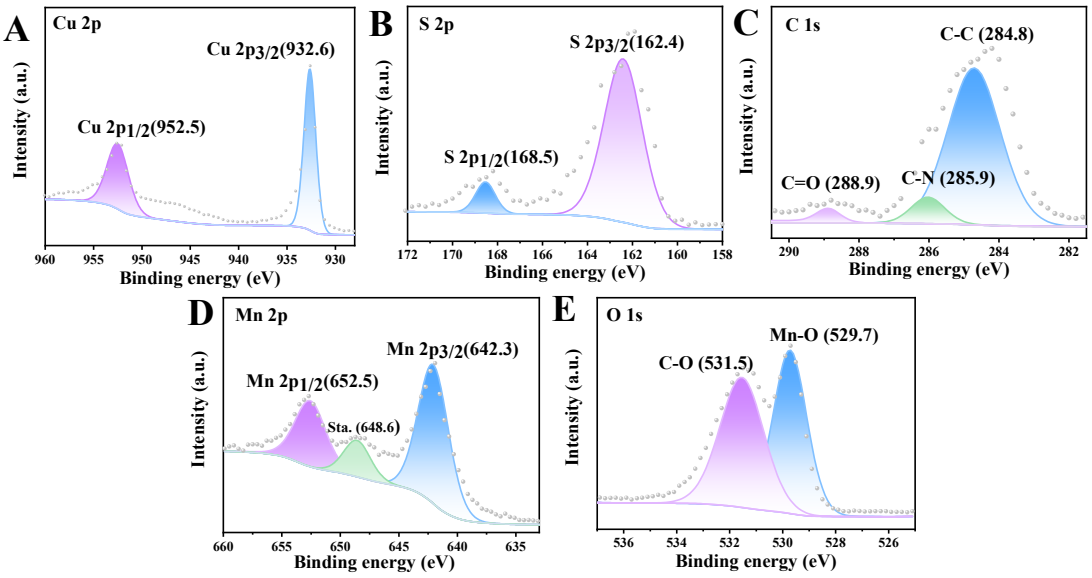

Fig. S2. XPS spectrum of Cu 2p (A), S 2p (B), C 1s (C), Mn 2p (D) and O 1s (E) for CuS-CDs@MnO_2.

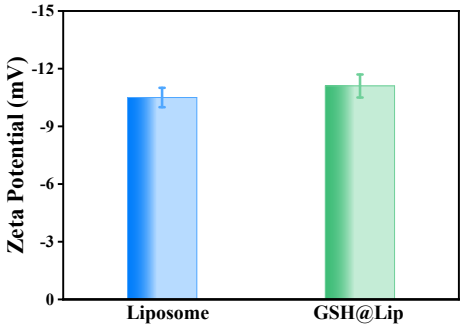

Fig. S3.Zeta potential plots of GSH and GSH@Lip

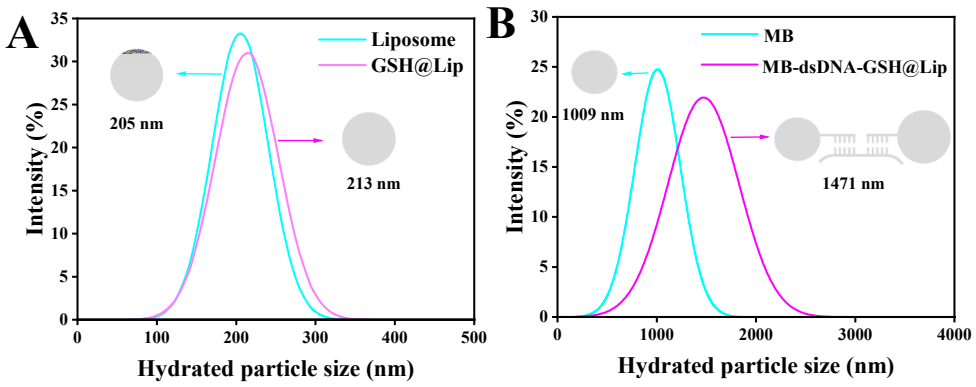

Fig. S4. (A) DLS data of Liposome and GSH@Lip; (B)DLS data of MB and MB+dsDNA+GSH@Lip.

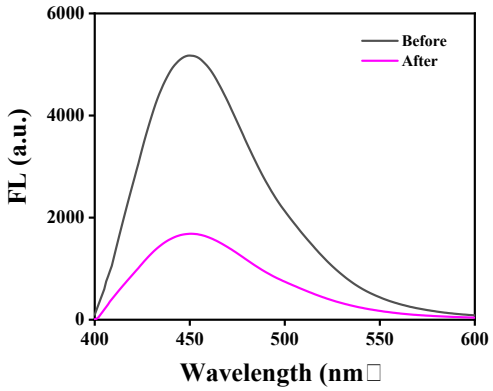

Fig. S5. Fluorescence spectra of the GSH solution reacting with CuS-CDs@MnO_2 before and after being loaded into the liposome suspension. Based on the fluorescence intensity at 450 nm, the loading efficiency was calculated to be 67.44% using the following formula:

Encapsulation efficiency = (Total GSH – Unloaded GSH) / Total GSH × 100%.

The calculation for amount of GSH per liposome

(1) The average head group surface area per lipid molecule:

$A = A1P1 + A2P2 + A3P3 = 0.475 \times 0.72 + 0.468 \times 0.19 + 0.0566 \times 0.5 = 0.4592\ nm^2$

(2) The number of lipids per liposome:

$N_{tot} = 4\pi [R^2 + (R - T)^2]/A = 4\pi [102.5^2 + (102.5 - 4)^2]/0.4592 = 5.53 \times 10^5$

(3) The number of liposomes per L:

$N_{lip} = (M_{lipid} \times N_A)/N_{tot} = (8.84 \times 10^{-6} \times 6.02 \times 10^{23})/5.53 \times 10^5 = 9.62 \times 10^{12}$

(4) Assuming that the GSH concentration inside the liposomes (M_{lipid}) is identical to the original solution used , the amount of GSH per liposome was calculated as follows:

$$N_{GSH} = (M_{lipid} \times N_A)/N_{lipld} = (0.1\times2\times10^{-3} \times 6.02 \times 10^{23})/9.62 \times 10^{12} = 1.25 \times 10^{7}$$

Where R is the diameter size of GSH@Lip from TEM measurements, A is the average head group surface area per lipid, and T is the bilayer thickness (4 nm). The components in the lipid composition are taken into account to theoretically calculate the average head group surface area per lipid (A). A1, A2, and A3 are 0.342 nm², 0.0889 nm², and 0.0283 nm² for DOPC, cholesterol, and DSPE-PEG-Mal, respectively. P1, P2, and P3 are the mole fractions of DOPC, cholesterol, and DSPE-PEG-Mal, respectively. The A obtained for these liposomes is 0.4592 nm² through using these values and weighting by the mole fraction of each component. N_{tot} is the number of lipids per liposome, N_{lipid} is the number of liposomes per L, and M_{lipid} means the molar concentration of lipid.

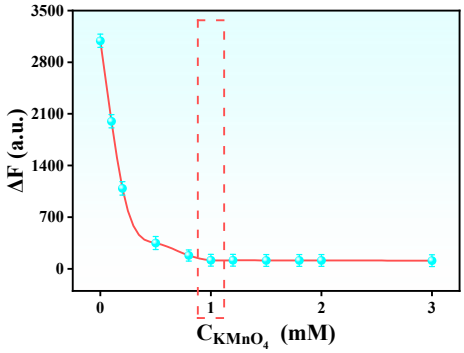

Fig. S6. Fluorescence intensity changes of CuS-CDs with different concentrations of $KMnO_4$.

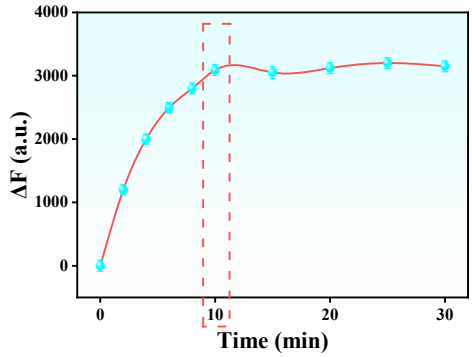

Fig. S7. Time-dependent fluorescence intensity of CuS-CDs@MnO_2 at 450 nm in the presence of 1 mM GSH.

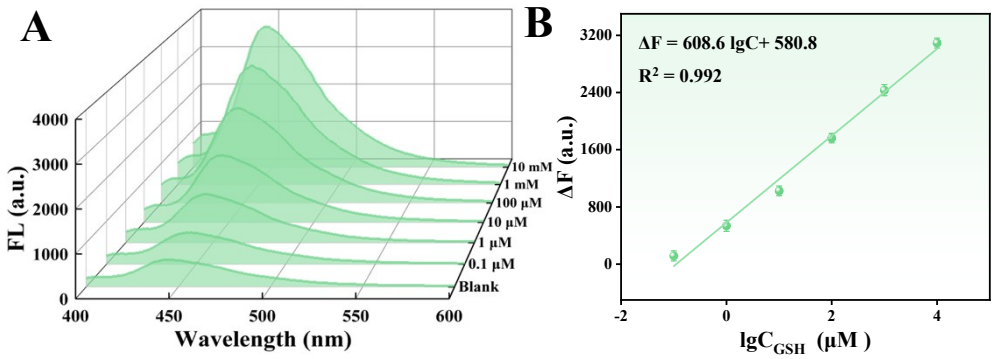

Fig. S8. (A) Fluorescence spectra of CuS-CDs@MnO_2 at different GSH concentrations; (B) Correlation between fluorescence intensity and the logarithm of GSH concentration.

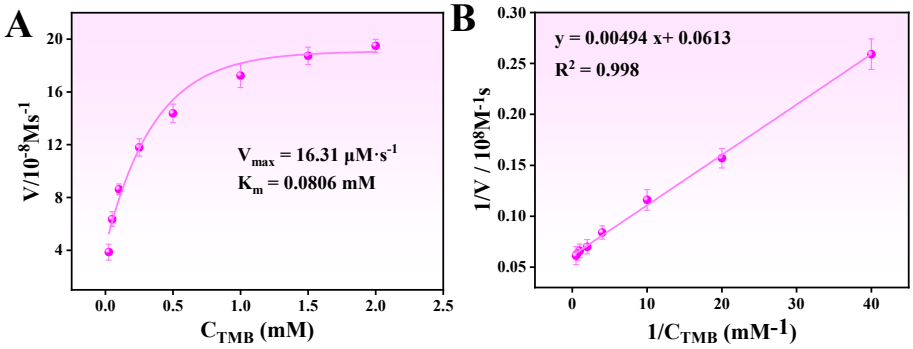

Fig. 9. (A) Lineweaver-Burk plot of CuS-CDs@MnO_2 for TMB; (B) Double reciprocal plot of the initial reaction rate of CuS-CDs@MnO_2 for TMB.

Table S2. The Km and Vmax values of the CuS-CDs@MnO_2 and other oxidase-like catalysts for the substrate of TMB.

Materials	Km (mM)	Vmax (10^{-8} M S^{-1})	Ref.
CuNPs/CoO/CNFs	0.26	12.32	[55]
OVs-Mn_2O_3-400	0.149	10.44	[56]
DSNCs	0.48	5.32	[57]
Pd@PtNPs	0.50	1.50	[58]
ZnCu100H	1.81	9.02	[59]
RhNPs	0.78	16.26	[60]
Pd@IrNPs	0.42	1.88	[61]
HRP	0.43	10	[62]

CuS-CDs@MnO_2	**0.0806**	**16.31**	**This work**

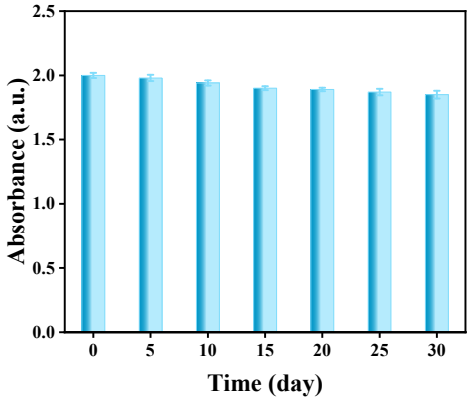

Fig. S10. Oxidative enzyme catalytic stability of CuS-CDs@MnO_2.

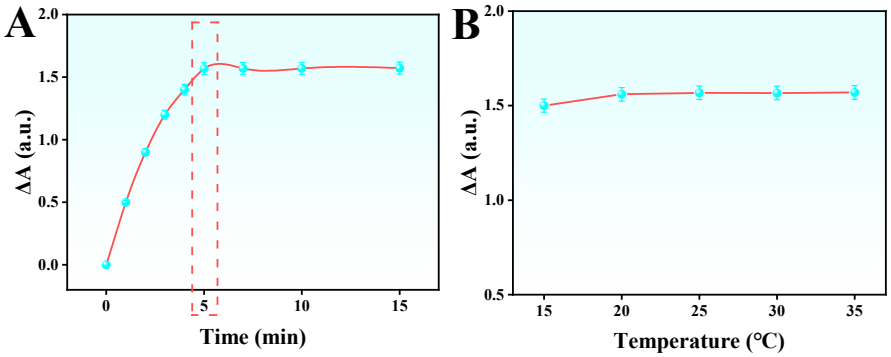

Fig. S11. (A) The effect of reaction time on the oxidase activity of TMB and CuS-CDs@MnO_2; and (B) the effect of temperature on the oxidase activity.

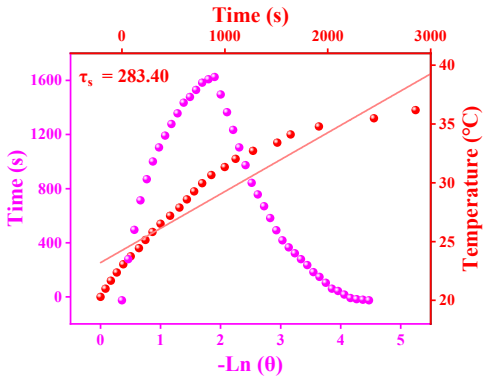

Fig. S12. Temperature variation diagram of photothermal-cooling of CuS-CDs@MnO_2 and the relationship diagram between time and the negative natural logarithm of the temperature increment during cooling cycles.

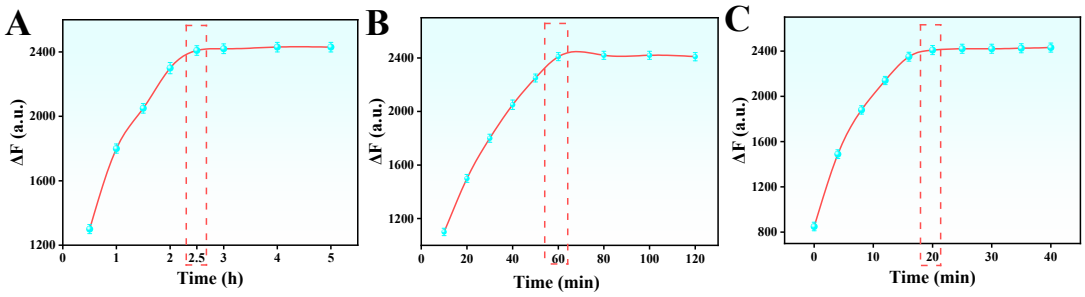

Fig. S13. Optimization of experimental conditions: (A) dsDNA hybridization time; (B) Aptamer-target reaction time; (C) Reaction time of the Supernatant with the CuS-CDs@MnO_2 system.

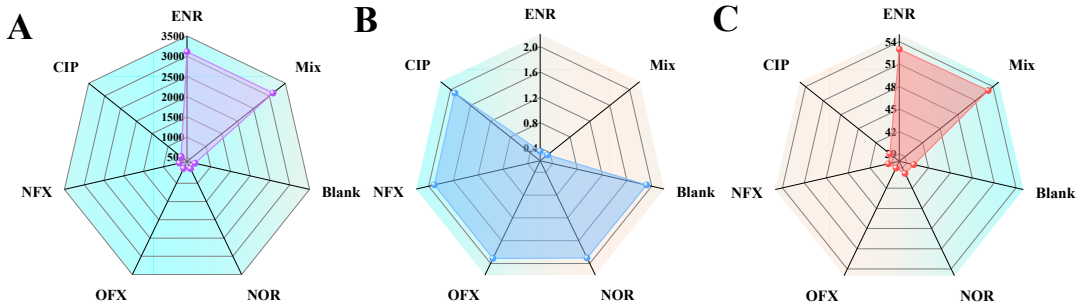

Fig. S14. Selectivity of (A) fluorescent, (B) colorimetric, and (C) photothermal sensors. (The concentration of ENR was 10 μg/ml, and the concentration of interferants was 100 μg/ml).

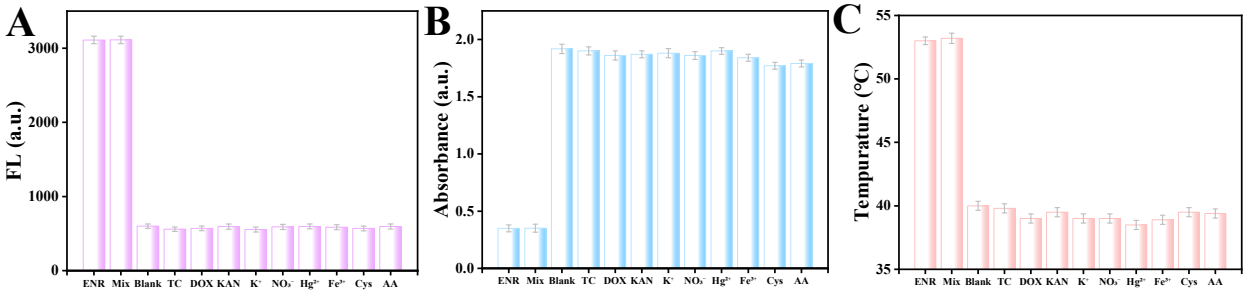

Fig. S15. Selectivity of (A) fluorescent, (B) colorimetric, and (C) photothermal sensors.

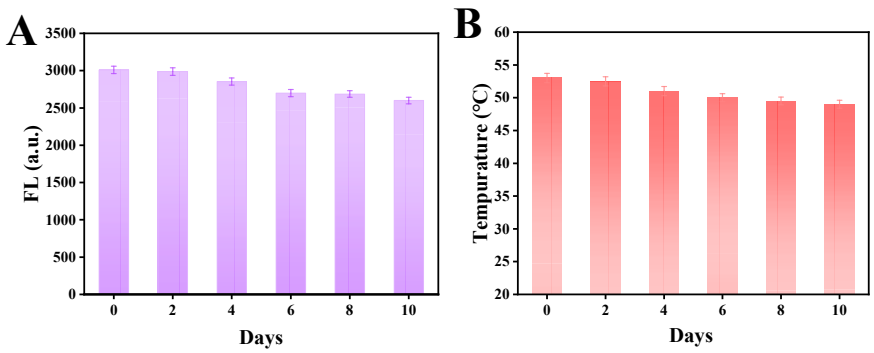

Fig. S16. Stability of (A) fluorescent and (B) photothermal sensors.

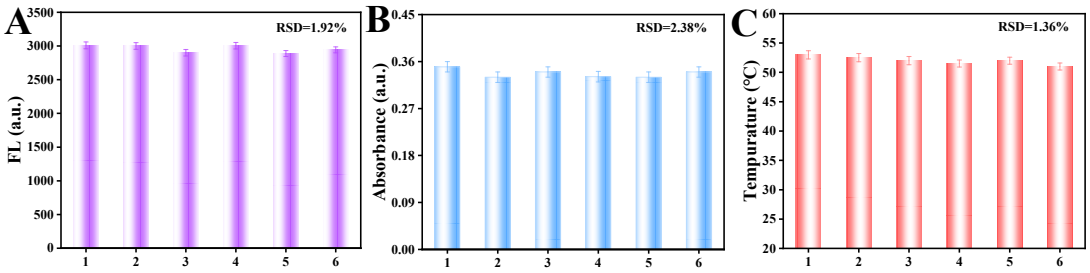

Fig. S17. Reproducibility of (A) fluorescent, (B) colorimetric, and (C) photothermal sensors.

Table S3. Comparison of different methods for ENR detection

Analytical method	Materials and strategy	Linear range ($\mu g \cdot mL^{-1}$)	Detection limit ($\mu g \cdot mL^{-1}$)	Refs.
FL	Fluorescent sensor with N-CDs-Cu^{2+}	1.0–15.0	0.16	[63]
Photothermal	Biosensor with MGO@Au@Ab-DITS	25−1000	10.89	[64]
Colorimetric	Biosensor with MGO@Au@Ab-DITS	25−1000	23.05	[64]
FL	Fluorescent sensor with fluorophore	0–1.478	0.133	[65]
FL	Fluorescent sensor with AIS QDs	0.3125–20.00	0.024	[66]
FL	Fluorescent sensor with AgNPs	0.05–0.6	0.021	[67]
FL	Fluorescent sensor with G-CDs/AuNPs	1–50	0.04	[68]
FL	**Tri-mode aptasensor with CuS-**	**0.001–10**	**0.000543**	**This**

	CDs@MnO_2			**work**
Colorimetric	**Tri-mode aptasensor with CuS-CDs@MnO_2**	**0.001–10**	**0.00706**	**This work**
Photothermal	**Tri-mode aptasensor with CuS-CDs@MnO_2**	**0.001–10**	**0.0302**	**This work**

Table S4 Detection of actual samples for ENR

sample	Added ($\mu g \cdot mL^{-1}$)	Fluorometric mode			Colorimetric mode			Photothermal mode		
		Found ($\mu g \cdot mL^{-1}$)	Recovery (100 %)	RSD (%,n=3)	Found ($\mu g \cdot mL^{-1}$)	Recovery (100 %)	RSD (%, n=3)	Found ($\mu g \cdot mL^{-1}$)	Recovery (100 %)	RSD (%, n=3)
Milk	0.1	0.097	97.0	2.14	0.108	108.3	3.89	0.094	94.0	3.45
	1	0.986	98.6	1.75	1.044	104.4	2.59	0.963	96.3	2.42
	10	10.091	100.9	1.55	10.272	102.7	2.15	9.787	97.8	2.17
Lake water	0.1	0.103	103.0	2.42	0.092	92.0	3.83	0.109	108.9	4.01
	1	1.022	102.2	2.01	0.957	95.7	2.82	1.062	106.2	3.37
	10	9.876	98.76	1.70	10.183	101.8	2.14	9.612	96.1	2.54

Large files may prove difficult for users to download and access

References cited in the Supplementary Information (SI) may be listed at the bottom of the reference section of the main manuscript. Please include a note in the data availability statement to explain that references cited in the SI have been listed in the article’ s reference list. Here is an example of how this could be presented: References 55-68 are cited in the Supplementary information (SI).